Geophys. J. Int. (2009) **178,** 375–393 doi: 10.1111/j.1365-246X.2009.04144.x

Transient solution for poro-viscoacoustic wave propagation in double porosity media and its limitations

Xu Liu,[1] Stewart Greenhalgh[1,2] and Bing Zhou[1]

[1]*Department of Physics, University of Adelaide, North Terrace Campus,* ADELAIDE SA 5005*, Australia. E-mail: xu.liu@adelaide.edu.au*
[2]*Institute of Geophysics, ETH Zürich, Zürich,* 8092 CH *Switzerland*

Accepted 2009 February 9. Received 2009 February 4; in original form 2008 December 3

SUMMARY

The analytical transient acoustic solution and dispersion characteristics for the double-porosity model are obtained over the whole frequency range for a homogeneous medium. The solution is also obtained by approximating the double porosity model with a uniform poro-viscoacoustic model and then constructing the transient response. The comparison between the results of the two models shows the likely validity and limitations of numerical solutions using a poro-viscoacoustic model to represent a double porosity medium in the heterogeneous case. Our calculations show that the dissipation by local mesoscopic flow of the double porosity model is very hard to fit over the entire frequency range by a single Zener element. However, since seismic exploration is normally restricted to a fairly narrow frequency band, this means that for frequency-dependent material properties, such as attenuation, the values around the centre frequency of the source will primarily determine the wave propagation characteristics. We choose the relaxation function that just approximates the dispersion behaviour of the double porosity model around the source centre frequency. It is shown that if the frequency is much lower than the peak attenuation frequency of the double porosity model, then wave propagation can be well described by the poro-viscoaoustic model with a single Zener element. For most water-filled sandstones having a double porosity structure, this holds true across the seismic frequency range. The transient solution for the heterogeneous double porosity medium is numerically obtained by a time splitting and Fourier pseudo-spectral staggered-grid method. As illustrative examples, the 2-D wavefield in a two-layer, water-saturated double porosity model are approximated by poro-viscoacoustic and poro-viscoelastic methods, respectively.

Key words: Numerical solutions, Elasticity and anelasticity; Seismic attenuation; Wave propagation.

1 INTRODUCTION

It is well known that Biot theory (Biot 1956, 1962) of porous-media acoustics ignores all wave-induced flow at mesoscopic scales, that is, scales greater than the grain size but less that the wavelength. Biot's theory used in homogeneous media cannot explain the high level of attenuation observed in natural porous media such as fluid-filled sands or sandstone over the seismic frequency range (10–200 Hz). This attenuation is successfully described by the mesoscopic heterogeneity models (e.g. White 1975; Dutta & Odé 1979a,b; Gurevich & Lopatnikov 1995; Gelinksy & Shapiro 1997; Johnson 2001; Carcione 2007). By applying the volume averaging theory to the local Biot poroelastic law, Pride & Berryman (2003a,b) developed the double-porosity, dual permeability (DPDP) model. It provides a theoretical framework, including the field equations governing the linear acoustics of composites with two isotropic porous constituents (phase 1 and phase 2), to model acoustic wave propagation through heterogeneous porous structures. In simple terms, it is an internal fluid transfer model, which is introduced to describe the flow between phase 1 and phase 2 in this theory, which provides an important energy dissipation mechanism for explaining the high attenuation at seismic frequencies. Unlike Darcy's fluid flux, the internal transport is a mesoscopic scale flow, which does not depend on the pore pressure gradient but the difference between the average fluid pressures. Pride *et al.* (2004) show that this theory can also be designed to approximate the patchy-saturation model (Johnson 2001) and the squirt-flow model (Dvorkin *et al.* 1994), which explain attenuation at ultrasonic frequencies. Under the assumption that phase 2 is entirely embedded in phase 1, the double-porosity theory is reduced to the effective Biot theory with complex frequency-dependent elastic moduli, through which the internal mesoscopic flow is incorporated. This theory provides good agreement with actual measurements of

attenuation over the seismic and ultrasonic frequency bands (Pride *et al.* 2004). However, this theory is limited to isotropic macroscopic media.

In this paper, we refer to the effective Biot theory as the double porosity theory. Obviously, double porosity theory not only provides a more general model to describe the attenuation mechanism but also the governing equations to calculate the averaged wave fields in porous media having mescoscopic heterogeneities. Otherwise, it is very difficult to numerically model a macroscopic wave in a porous medium (of dimensions hundreds to thousands of metres), having mescoscopic heterogeneities (with a size of several millimeters).

Carcione & Quiroga-Goode (1996) analytically solved the Biot acoustic field equations in homogeneous porous media in the frequency domain and then applied an inverse Fourier transformation to get the waveform in the time domain. Comparing the governing equations of the double porosity theory with those of Biot theory, we find the only difference is that the moduli of the double porosity theory are complex and frequency-dependent. The similarity between the two theories implies that the field equations of the double porosity theory can be solved analytically in homogeneous double porosity media, in both the frequency and the time domains. Here, the word 'homogeneous' means at the macroscopic level. The analytical solution is very important for understanding the influence of the material properties of double porosity media. This includes the effects of poroelastic mechanics of the host material (phase 1), the volume fraction and size of inclusions of phase 2, the fluid viscosity, etc. on the velocity and the inverse quality factor (attenuation) of the composite medium. Furthermore, the analytical solutions provide a means of checking the numerical simulation of waves in double porosity media.

It is very difficult to analytically solve the field equations in heterogeneous double porosity media. This requires a numerical approach. Although there are several methods to numerically solve the wave equations, like the finite element method and the finite difference method (see the review article by Carcione *et al*. 2002), wave propagation in fluid-filled porous medium presents special difficulties for modelling because of the interaction between the solid frame and the pore fluid. For example, the equations are stiff and the moduli are frequency-dependent. This implies energy dissipation, and the solutions should be expressed as convolution integrals in the time domain. It is worth briefly reviewing some numerical approaches for modelling waves in porous media.

The presence of the Biot slow *P* wave makes Biot's differential equation stiff at low frequencies (Carcione & Quiroga-Goode 1995), since the slow *P* wave is actually diffusive, having a very small wavelength whereas the normal or fast *P* wave has a large wavelength. Thus, it is very difficult to choose an appropriate time step for both *P* waves. To circumvent this difficulty, Carcione & Quiroga-Goode (1995) partitioned the governing equation into two sets of differential equations, one stiff and the other non-stiff. The splitting technique is to solve the stiff part analytically and then the non-stiff part by the fourth-order Runge-Kutta algorithm. Two energy dissipation mechanisms have been well described by the standard linear solid or Zener model, which allows the convolution integral to be replaced by memory equations (according to Carcione 1996, 1998). One refers to Biot's viscodynamic operators in the high frequency range, or the Biot mechanism, and the other denotes squirt flow. Since the Biot attenuation mechanism is not related to bulk deformation, the Zener model, which generalizes compressibility to a relaxation function, is not appropriate to describe the Biot complex moduli (see Carcione 1998). Instead, the compressional wave attenuation and velocity dispersion are matched directly by using relaxation functions associated with each wave mode (Carcione 1996, 1998). Carcione (1998) also shows that a homogeneous porous medium can actually be modelled by a single-phase viscoelastic medium and that only one relaxation mechanism (or Zener relaxation function) for each viscoelastic modulus is enough to describe the moduli of the porous medium.

In parallel with the above issue are the questions as to whether the internal mesoscopic flow model can be represented by one Zener element, and how one should solve for wave propagation in heterogeneous double porosity media. To the best of our knowledge, there is no paper providing solutions to the wavefields in heterogeneous, double porosity media. However, the current double porosity model (Pride *et al.* 2003, 2004) does not include the shear wave response. It is acoustic response only. There is no current analytic model describing shear wave energy attenuation due to mesoscopic inhomogeneities in fluid-saturated porous medium. Some experiments (Jones 1986) show that the intrinsic attenuation of shear waves could be of a similar magnitude to that of compressional waves in fluid saturated porous media. This means that acoustic wave modelling is not realistic. Therefore, we apply a poro-viscoelastic approach to compensate for this deficiency. As a special case of poro-viscoelasticity with zero shear response, the poro-viscoacoustic approach can be compared with the analytical (acoustic) solution of double porosity theory to assess its validity and limitations.

In this paper, we first derive the phase velocity and the specific quality factor dispersion relations for the double porosity model and the poro-viscoacoustic model in which the complex modulus matrix is replaced with a Zener relaxation function. We then develop an analytic transient wave field solution for both models under the acoustic approximation, which allows a comparison of the phase velocity and intrinsic attenuation between the two models. Finally, the 2-D wavefield in a two-layer, water-saturated double porosity model are approximated by poro-viscoacoustic and poro-viscoelastic methods, respectively.

2 THE ANALYTICAL SOLUTION FOR A HOMOGENEOUS MEDIUM

2.1 Double porosity model

The double porosity model (or effective single-porosity Biot theory developed by Pride *et al.* 2003, 2004) includes constitutive equations, the linear transport law and the linear momentum conservation law. Under a time dependence ofe $^{-i\omega t}$, the frequency-domain constitutive

equations are

$$\frac{1}{\mathrm{i}\omega}\begin{bmatrix}\nabla\cdot\mathbf{v}\\ \nabla\cdot\mathbf{q}\end{bmatrix}=\begin{bmatrix}a_{11}^{*} & a_{12}^{*}\\ a_{12}^{*} & a_{22}^{*}\end{bmatrix}\begin{bmatrix}p_{\mathrm{c}}\\ p_{\mathrm{f}}\end{bmatrix}, \tag{1}$$

$$\nabla\mathbf{v}+(\nabla\mathbf{v})^{T}-\tfrac{2}{3}\nabla\cdot\mathbf{v}\mathbf{I}=-i\omega\boldsymbol{\sigma}^{D}\big/[G(\omega)-\mathrm{i}\omega g(\omega)]. \tag{2}$$

Here $\mathbf{v}$ is the average particle velocity of the solid grains, $\mathbf{q}$ is the macroscopic fluid flux through phase 1, p_{c} is the average total pressure, p_{f} is the average fluid pressure within phase 1. $\boldsymbol{\sigma}^{\mathrm{D}}$ is the average viscous deviatoric stress tensor acting on the solid grains; it is defined as $\boldsymbol{\sigma}^{\mathrm{D}}=\boldsymbol{\sigma}-p_{\mathrm{c}}\mathbf{I}$, where $\boldsymbol{\sigma}$ and $\mathbf{I}$ represent the average total stress tensor and the second-order unit tensor respectively; $G(\omega)$ and $g(\omega)$ are both real functions that are Hillbert transforms of each other. At the low-frequency limit, $G(\omega)$ corresponds to the drained-shear modulus of the composite. The coefficients $a_{mn}^{*}(m, n = 1, 2)$depend on material parameters and frequency ω. They are listed in Appendix A. However, the DPDP model to date is entirely acoustic and, so, $G(\omega)$ and $g(\omega)$are not given in Appendix A.

The linear transport law can be stated as

$$\nabla p_{\mathrm{f}}=\mathrm{i}\omega\rho_{\mathrm{f}}\mathbf{v}-\frac{\eta}{\kappa^{*}(\omega)}\mathbf{q}, \tag{3}$$

where ρ_{f} and η are the density and the viscosity of the pore fluid, respectively, and $\kappa^{*}(\omega)$ is the dynamic permeability of the composite medium. Pride *et al.* (2003a, 2004) suggested taking the harmonic mean of the constituents as the best way to approximate it:

$$\frac{1}{\kappa^{*}(\omega)}=\frac{1-\nu_{2}}{\kappa_{1}(\omega)}+\frac{\nu_{2}}{\kappa_{2}(\omega)}. \tag{4}$$

Here, $\kappa_{1}(\omega)$and $\kappa_{2}(\omega)$ are the dynamic permeabilities (Johnson *et al.* 1987) of phase 1 and phase 2, respectively, whereas $\nu_{2}$is the volume fraction of phase 2.

The conservation of linear momentum equation is expressed as

$$\nabla\cdot\boldsymbol{\sigma}^{\mathrm{D}}-\nabla p_{\mathrm{c}}=-i\omega\left(\rho\mathbf{v}+\rho_{\mathrm{f}}\mathbf{q}\right), \tag{5}$$

where ρ is the total average density of the composite.

Eqs(1)–(3) and (5) are the governing equations in the frequency-domain for the double porosity model with a fully embedded phase 2.

Since the analytic transient solution can be easily obtained for the acoustic case, we firstly set to zero the shear response in the above equations. The acoustic wave dispersion characteristics are also easily obtained. Taking the divergence of eqs.(3) and (5), combining with eq.(1), eliminating the $\mathbf{v}$ and $\mathbf{q}$ terms, and adding in a source force term $\mathbf{S}$, we obtain

$$\boldsymbol{\Delta}\left(\mathbf{P}-\mathbf{S}\right)+\omega^{2}\mathbf{D}\cdot\mathbf{P}=0, \tag{6}$$

where

$$\mathbf{P}=\begin{bmatrix}p_{\mathrm{c}}\\ p_{\mathrm{f}}\end{bmatrix},\ \mathbf{S}=\begin{bmatrix}S\\ S_{\mathrm{f}}\end{bmatrix}\text{ and }\mathbf{D}=\boldsymbol{\Gamma}\cdot\mathbf{M}, \tag{7}$$

with

$$\boldsymbol{\Gamma}=\begin{bmatrix}\rho & \rho_{\mathrm{f}}\\ \rho_{\mathrm{f}} & -\frac{\eta}{\mathrm{i}\omega\kappa^{*}(\omega)}\end{bmatrix},\ \mathbf{M}=\begin{bmatrix}a_{11}^{*} & a_{12}^{*}\\ a_{12}^{*} & a_{22}^{*}\end{bmatrix}. \tag{8}$$

Comparing eq. (6) with eq. (26) in the paper by Carcione & Quiroga-Goode (1996), we find that there are some differences. On one hand the a_{ij}^{*} elements of the $\mathbf{M}$ matrix are complex frequency-dependent values (see Appendix A), whereas the corresponding elements in Carcione's eq. (26) are real values. On the other hand, the effective permeability $\kappa^{*}(\omega)$ in the $\boldsymbol{\Gamma}$ matrix of eq. (8) is defined by eq. (4), and it's frequency response depends on the combined response of both porous phases following the Johnson model (Johnson *et al.* 1987). Eq. (4) is assumed to hold true over the full frequency range (low and high frequencies), whereas Carcione & Quiroga-Goode (1996) use the simplification of $\frac{\eta}{\kappa^{*}(\omega)}$, given by Biot (1962b) at low frequency and that given by Auriault *et al.* (1985) at high frequency, respectively. Following their approach, eq. (6) can be solved to get the characteristic equation

$$\det\left[\mathbf{D}-\left(\frac{k}{\omega}\right)^{2}\mathbf{I}\right]=0, \tag{9}$$

where $k=|\mathbf{k}|$, and $\mathbf{k}$ is the complex wavevector. The eigenvalues of $\mathbf{D}$ are given by

$$\lambda_{1(2)}=\frac{1}{2}\left[U\pm\sqrt{U^{2}-4\det\mathbf{M}\det\boldsymbol{\Gamma}}\right] \tag{10}$$

and

$$U=\rho a_{11}^{*}+2\rho_{\mathrm{f}}a_{12}^{*}-\frac{\eta}{\mathrm{i}\omega\kappa^{*}}a_{22}^{*}. \tag{11}$$

The complex velocities are given by

$$V_{v}=\frac{1}{\sqrt{\lambda_{v}}},\qquad v=1,2, \tag{12}$$

where $v = 1, 2$ corresponds to the fast and the slow P waves, respectively.

The phase velocities c_v and quality factors Q_v can be expressed as

$$c_v(\omega) = \left(\mathrm{Re}\left[\frac{1}{V_v} \right] \right)^{-1} \text{and} Q_v(\omega) = \frac{\mathrm{Re}\left[V_v^2\right]}{\mathrm{Im}\left[V_v^2\right]}. \tag{13}$$

The slow wave is very difficult to measure because of the extremely high attenuation. In this paper, we focus on the fast wave.

Following Carcione & Quiroga-Goode (1996) and Carcione (2007), the transient solution of (6) is shown to be

$$\mathbf{P} = G(\mathbf{D}) \cdot \mathbf{S}h(\omega), \tag{14}$$

where

$$G(\mathbf{D}) = \frac{1}{\lambda_1 - \lambda_2} \left\{ [G(\lambda_1) - G(\lambda_2)]\, \mathbf{D} + [\lambda_1 G(\lambda_2) - \lambda_2 G(\lambda_1)]\, \mathbf{I} \right\}, \tag{15}$$

$$G(\lambda_v) = -\left[\omega^2 \lambda_v g(\lambda_v) + 8\delta(\mathbf{x}) \right] v = 1, 2, \tag{16}$$

$$\begin{cases} g(\lambda_v) = -2\mathrm{i} H_0^{(2)} \left[\omega r \sqrt{\lambda_v(\omega)} \right] \\ r = \sqrt{x^2 + z^2} \end{cases} \text{for the 2D solution (line source),} \tag{17}$$

$$\begin{cases} g(\lambda_v) = \frac{1}{r} \exp\left[-\mathrm{i}\omega r \sqrt{\lambda_v(\omega)} \right] \\ r = \sqrt{x^2 + y^2 + z^2} \end{cases} \text{for the 3D solution (point source).} \tag{18}$$

Here $H_0^{(2)}$ is the Hankel function of the second kind, $\mathbf{S} = [\mathrm{S}, \mathrm{S_f}]$ is a constant vector and set as $\mathbf{S} = [1, 1]$ in this paper, whereas $h(\omega)$ represents the source frequency spectrum.

The analytical solution in the time domain can be obtained by an inverse Fourier transformation.

For the following example, we choose the source to be a Ricker wavelet time function (from Carcione & Quiroga-Goode 1995):

$$f(t) = \exp\left[-\frac{1}{2} f_c^2 (t - t_0)^2 \right] \cos\left[\pi f_c (t - t_0) \right], \tag{19}$$

where $t_0 = 3/f_c$ and f_c is the centre frequency.

To compare with the numerical solutions in the following sections, the source term in eq. (14) should be written as

$$h(\omega) = \frac{F(f(t))}{\mathrm{i}\omega}, \tag{20}$$

where $F(f(t))$ means the Fourier transform of $f(t)$.

2.2 Poro-viscoacoustic model

Based on the double porosity model, the poro-viscoacoustic model is obtained by replacing the complex modulus in the constitutive equations by the viscoacoustic model (Carcione 2007).

Eq.(1) can be rewritten as

$$\mathrm{i}\omega \begin{bmatrix} p_c(\omega) \\ p_f(\omega) \end{bmatrix} = \begin{bmatrix} a_{11}^{-*}(\omega) & a_{12}^{-*}(\omega) \\ a_{12}^{-*}(\omega) & a_{22}^{-*}(\omega) \end{bmatrix} \begin{bmatrix} \nabla \cdot \mathbf{v}(\omega) \\ \nabla \cdot \mathbf{q}(\omega) \end{bmatrix}, \tag{21}$$

where $a_{ij}^{-*}(\omega)$ is the complex modulus matrix and equal to the inverse of matrix $a_{ij}^{*}(\omega)$. The general form of eq. (21) can be rewritten in terms of relaxation functions ψ_{mn} (m,n = 1,2) in the time domain as

$$-\begin{bmatrix} \dot{p}_c(t) \\ \dot{p}_f(t) \end{bmatrix} = \begin{bmatrix} \dot{\psi}_{11}(t) & \dot{\psi}_{12}(t) \\ \dot{\psi}_{21}(t) & \dot{\psi}_{22}(t) \end{bmatrix} * \begin{bmatrix} \nabla \cdot \mathbf{v}(t) \\ \nabla \cdot \mathbf{q}(t) \end{bmatrix}. \tag{22}$$

Here $*$ denotes time convolution. This equation is obtained by assuming homogeneous media; therefore the simulation based on the equation has this approximation.

The Fourier transform of eq. (22) is:

$$i\omega \begin{bmatrix} p_c(\omega) \\ p_f(\omega) \end{bmatrix} = \begin{bmatrix} F(\dot{\psi}_{11}) & F(\dot{\psi}_{12}) \\ F(\dot{\psi}_{21}) & F(\dot{\psi}_{22}) \end{bmatrix} \begin{bmatrix} \nabla \cdot \mathbf{v}(\omega) \\ \nabla \cdot \mathbf{q}(\omega) \end{bmatrix}, \tag{23}$$

where F denotes Fourier transformation.

We use the Zener model to represent the relaxation functions and investigate the discrepancy between this replacement and the double porosity model.

The relaxation functions of the Zener model are given by Carcione (1996, 2007) as

$$\psi_{mn} = \breve{\psi}_{mn} H(t), \tag{24}$$

where $H(t)$ refers to the Heaviside (unit step) function, and

$$\breve{\psi}_{mn} = \psi_{mn}(t=\infty)\left[1 - \frac{1}{L_{mn}}\sum_{l=1}^{L_{mn}}\left(1 - \frac{\tau_{mn}^{\varepsilon l}}{\tau_{mn}^{\sigma l}}\right)\exp\left(-\frac{t}{\tau_{mn}^{\sigma l}}\right)\right]. \tag{25}$$

In equ 2.24 $\psi_{mn}(t=\infty)$ are the values of the relaxation function at infinite time, which will determine the velocity of propagation; L_{mn} is the number of standard linear solid elements or Zener elements of ψ_{mn}; $\tau_{mn}^{\varepsilon l}$ and$\tau_{mn}^{\sigma l}$ are the relaxation times of the average particle velocity and the average stress of the solid phase, which will determine the attenuation property.

The Fourier transform $F(\dot{\psi}_{mn})$ is

$$F(\dot{\psi}_{mn}) = \frac{\psi_{mn}(t=\infty)}{L_{mn}}\sum_{l=1}^{L_{mn}}\frac{1 - \mathrm{i}\omega\tau_{mn}^{\varepsilon l}}{1 - \mathrm{i}\omega\tau_{mn}^{\sigma l}}. \tag{26}$$

Inserting eq. (26) into eq. (23) and comparing with (21) we find that:

$$a_{mn}^{-*}(\omega) = F(\dot{\psi}_{mn}) \tag{27}$$

or

$$a_{mn}^{-*}(\omega) = \frac{\psi_{mn}(t=\infty)}{L_{mn}}\sum_{l=1}^{L_{mn}}\frac{1 - \mathrm{i}\omega\tau_{mn}^{\varepsilon l}}{1 - \mathrm{i}\omega\tau_{mn}^{\sigma l}}. \tag{28}$$

Setting $\omega = 0$ and $\omega = \infty$ results in

$$a_{mn}^{-*}(\omega=0) = \psi_{mn}(t=\infty) \tag{29}$$

and

$$a_{mn}^{-*}(\omega=\infty) = \frac{\psi_{mn}(t=\infty)}{L_{mn}}\sum_{l=1}^{L_{mn}}\frac{\tau_{mn}^{\varepsilon l}}{\tau_{mn}^{\sigma l}}. \tag{30}$$

By eq. (25),

$$\psi_{mn}(t=0^{+}) = \frac{\psi_{mn}(t=\infty)}{L_{mn}}\sum_{l=1}^{L_{mn}}\frac{\tau_{mn}^{\varepsilon l}}{\tau_{mn}^{\sigma l}}. \tag{31}$$

This means

$$a_{mn}^{-*}(\omega=\infty) = \psi_{mn}(t=0^{+}). \tag{32}$$

Combining eqs (32), (29) and (31) gives,

$$a_{mn}^{-*}(\omega=\infty) = \frac{a_{mn}^{-*}(\omega=0)}{L_{mn}}\sum_{l=1}^{L_{mn}}\frac{\tau_{mn}^{\varepsilon l}}{\tau_{mn}^{\sigma l}}. \tag{33}$$

If the Zener model can fully describe the double porosity model, then both eq. (28) and (33) must be satisfied. However, as we will see the Zener element cannot fully represent the double porosity model. On the other hand, since all the field quantities of double porosity theory are defined as the volumetric average values, which require that the wavelength is larger than the size of mesoscopic heterogeneities, this assumption will not be valid for infinite (very large) frequency. In the following calculations, all terms $a_{mn}^{-*}(\omega=\infty)$should be replaced by $a_{mn}^{-*}(\omega=0)$through eq. (33).

Eqs (23), (5) and (3) are the governing equations of the poro-viscoacoustic model in the frequency domain.

Taking the divergence of eqs (5), (3), combining with eq. (23) and eliminating $\mathbf{v}(\omega)$ and $\mathbf{q}(\omega)$, we obtain the dispersion equation for homogeneous poro-viscoacoustic waves. It can be expressed by

$$\mathbf{\Delta}\begin{bmatrix} p_c \\ p_f \end{bmatrix} + \omega^2\begin{bmatrix} \rho & \rho_f \\ \rho_f & -\frac{\eta}{\mathrm{i}\omega\kappa^{*}(\omega)} \end{bmatrix}\begin{bmatrix} F(\dot{\psi}_{11}) & F(\dot{\psi}_{12}) \\ F(\dot{\psi}_{21}) & F(\dot{\psi}_{22}) \end{bmatrix}^{-1}\begin{bmatrix} p_c \\ p_f \end{bmatrix} = 0. \tag{34}$$

Adding in a source force term $\mathbf{S}$ to the above equation and rewriting it we get

$$\mathbf{\Delta}\,(\mathbf{P} - \mathbf{S}) + \omega^2\mathbf{\Gamma}\mathbf{N}^{-1}\mathbf{P} = 0, \tag{35}$$

where $\mathbf{S}$ and $\mathbf{\Gamma}$are defined in eqs (7) and (8). The other terms are defined by

$$\mathbf{P} = \begin{bmatrix} p_c \\ p_f \end{bmatrix} \text{and } \mathbf{N} = \begin{bmatrix} F(\dot{\psi}_{11}) & F(\dot{\psi}_{12}) \\ F(\dot{\psi}_{21}) & F(\dot{\psi}_{22}) \end{bmatrix}. \tag{36}$$

The eigenvalues $\hat{\lambda}_{1,2}$ of $\mathbf{\Gamma}\mathbf{N}^{-1}$ are given by

$$\hat{\lambda}_{1,2} = \frac{1}{2\det(\mathbf{N})}\left[\hat{U} \pm \sqrt{\hat{U}^2 - 4\det(\mathbf{\Gamma})\det(\mathbf{N})}\right] \tag{37}$$

and

$$\hat{U} = \rho F(\dot{\psi}_{22}) - \rho_f\left[F(\dot{\psi}_{21}) + F(\dot{\psi}_{12})\right] - F(\dot{\psi}_{11})\frac{\eta}{\mathrm{i}\omega\kappa^{*}(\omega)}. \tag{38}$$

Similarly, the transient solution of (35) can be obtained by replacing $\lambda_1$and λ_2 in (17) and (18) with $\hat{\lambda}_1$and $\hat{\lambda}_2$, respectively. The hat symbol '^' above λ implies the value of the poro- viscoacoustic model.

To fully represent the double porosity model means that the Zener elements should be chosen to make $\hat{\lambda}_{1,2} = \lambda_{1,2}$ over the whole frequency range. Carcione (1998) shows that just one relaxation mechanism is enough for characterising each dissipation mechanism of squirt-flow, or the Biot mechanism. However, in the double porosity model, because the local mesoscopic flow is included in the complex modulus, we try the same Zener model for the averaged movements **v** and **q** of both the solid frame and pore fluid. Therefore we assume a single Zener element with one set of relaxation times which means$\tau^{\varepsilon l}_{m1} = \tau^{\varepsilon l}_{m2} = \tau^{\varepsilon}and\tau^{\sigma l}_{m1} = \tau^{\sigma l}_{m2} = \tau^{\sigma}$. The relaxation times will be determined by the peak inverse quality factor $1/Q(f_{\mathrm{p}})$and the frequency $f_{\mathrm{p}}$of the double porosity model, in the following way:

$$\tau^{\varepsilon} = \frac{1}{2\pi f_{\mathrm{p}}}\left[\sqrt{Q^2(f_{\mathrm{p}})+1}+1\right] \text{and} \tau^{\delta} = \frac{1}{2\pi f_{\mathrm{p}}}\left[\sqrt{Q^2(f_{\mathrm{p}})+1}-1\right]. \tag{39}$$

3 VALIDITY AND LIMITATIONS

We now wish to examine the limitations and range of applicability of the poro-viscoacoustic model in double porosity media. We do so by means of specific examples. Two sample double porosity materials are denoted as Material A and Material B. Both materials have sandstone as the host rock (phase 1) and a volume fraction 3 per cent of sand as the inclusions (phase 2). Material A corresponds to a depth of 100 m and material B to a depth of 10 m according to Walton theory and the Hashin and Shtrikman bound (see Pride *et al.* 2004 for details). The material properties are listed in Table 1, and the physical meaning of the parameters is explained in Appendix A.

By means of eq. (13), the phase velocity $c(f_{\mathrm{p}})$ and attenuation $1/Q(f_{\mathrm{p}})$ dispersion curves of the double porosity model for materials A and B are computed and shown as the solid lines in Figs 1 and 2. In Fig. 1, for the material A, the peak inverse quality factor $1/Q(f_{\mathrm{p}})$ is 0.0437 ($Q \cong 23$) at a peak frequency f_{p} of 14 788 Hz, at which the phase velocity $c(f_{\mathrm{p}})$ is 2957 m s^{-1}. In Fig. 2, for material B, the peak value of $1/Q(f_{\mathrm{p}})$ is 0.0972 ($Q \cong 10$) and f_{p} is 4471 Hz, with a corresponding $c(f_{\mathrm{p}})$ of 2757 m s^{-1}. The peak frequency f_{p} refers to the frequency at which the mesoscopic structure just has time to equilibrate in one cycle.

The phase velocities $\hat{c}(f_{\mathrm{p}})$ and inverse quality factors $1/\hat{Q}(f_{\mathrm{p}})$of the visco-acoustic model can be obtained by inserting (39) into (26) and using $\hat{\lambda}_1$ in (37) to replace λ_1 in (12) and (13). The results are shown as the dashed lines in Figs 1 and 2 for homogeneous material A and B, respectively. They have the same peak frequency f_{p} as those of the solid lines.

Comparing the dashed line with the solid line in each figure reveals a significant discrepancy between the double porosity model and poro-viscoacoustic medium. Although the peak inverse quality factors $1/\hat{Q}(f_{\mathrm{p}})$ and $1/Q_{\mathrm{p}}$ are very similar around the peak frequency f_{p}, the phase velocity $\hat{c}$ is much different from c when the frequency is near f_{p}. This means that the dissipation mechanism of local flow of the double porosity model is very hard to be fit by one Zener element, which is inadequate to approximate the wave in the double porosity model over the whole frequency range.

However, the wave pulse used in field seismic exploration is usually at lower frequencies, less than several hundred hertz and has a relatively narrow band. This means that for frequency-dependent material properties, only the values around the centre frequency of the

Table 1. Material properties of the sample rocks and fluids.

Grain and fluid			
Parameter	Grains	Parameter	Water
K_s(N m^{-2})	$3.9 \times 10^{+10}$	K_f(N m^{-2})	2.25×10^9
G_s (N m^{-2})	$4.4 \times 10^{+10}$	ρ_f(kg m^{-3})	1000
ρ_s(kg m^{-3})	2650.0	η_f(kg m^{-1} s^{-1})	0.001

Materials A and B (corresponding to 100- and 10-m-depth double porosity sandstone)				
Parameter	Phase 1	Phase 2	Parameter	Composite
K_{dj}(N m^{-2})	2.23×10^{10}	6.45×10^8	K_d(N m^{-2})	1.41×10^{10}
	2.23×10^{10}*	2.04×10^{8}*		7.85×10^{9}*
G_{dj}(N m^{-2})	2.20×10^{10}	3.87×10^8	G_d(N m^{-2})	1.19×10^{10}
	2.20×10^{10}*	1.22×10^{8}*		5.98×10^{9}*
L1 (m)	0.0086	0.0086	ν_2	0.03
ϕ_j	0.20	0.36	ϕ	$\phi = (1-\nu_2)\phi_1 + \nu_2\phi_2$
κ_{0j}(m^2)	1.0×10^{-14}	1.0×10^{-9}	κ_0(m^2)	$1/\kappa_0 = (1-\nu_2/\kappa_{01} + \nu_2\kappa_{02}$
V/S (m)	0.005			

Note: The physical meaning of the various parameters is explained in Appendix A.
Subscript j denoting Phase 1 or 2
*implying material B

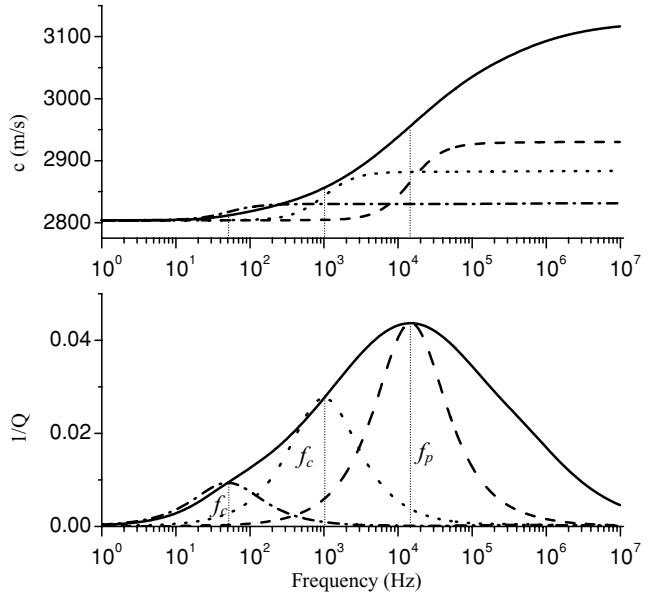

Figure 1. The dispersion curves of phase velocity c (upper) and inverse quality factor $1/Q$ (lower) for material A, which corresponds to water-filled double porosity sandstone at 100 m depth, and having a concentration of 3 per cent sand inclusions. The solid lines are the results for the double porosity model. The dashed lines, the dotted lines and the dash-dot lines are for porous-visco-acoustic material with a single relaxation function having a centre frequency of 50, 100 and 14 788 Hz (i.e. the peak attenuation frequency of the double porosity model), respectively.

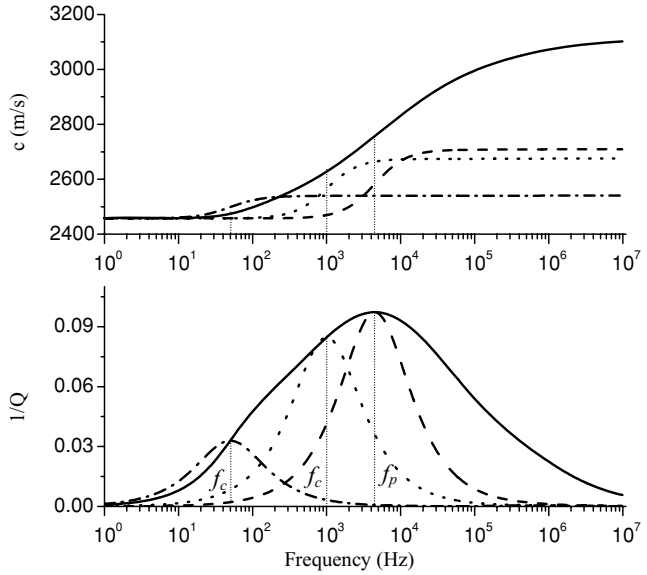

Figure 2. The dispersion curves of phase velocity (upper) and inverse quality factor (lower) for material B corresponding to water-filled double porosity sandstone at 10 m depth, and with a concentration of 3 per cent sand inclusions. The solid lines are the results for the double porosity model. The dashed lines, the dotted lines and the dash-dot lines are for porous-visco-acoustic material with a single relaxation function having a centre frequency of 50, 1000 and 4471 Hz (i.e. the peak attenuation frequency of the double porosity model), respectively.

seismic source f_{c} will determine the wave propagation. Therefore, we choose the relaxation function that just needs to approximate the dispersion behaviour of the double porosity model around f_{c}, which is also the peak frequency of the Zener element.

Now we use the dispersion curves of the double porosity model to determine the relaxation times of the poro-viscoacoustic model. By eq. (39) and replacing f_{p} with f_{c} and $1/Q(f_{\mathrm{p}})$ with $1/Q(f_{\mathrm{c}})$, we get

$$\tau^{\varepsilon} = \frac{1}{2\pi f_{\mathrm{c}}}\left[\sqrt{Q^2(f_{\mathrm{c}})+1}+1\right] \text{and} \tau^{\delta} = \frac{1}{2\pi f_{\mathrm{c}}}\left[\sqrt{Q^2(f_{\mathrm{c}})+1}-1\right]. \tag{40}$$

It should be noted that the phase velocity of the double porosity model $c(f_c)$ does not enter into the poro-viscoacoustic model, which actually depends on $c(f=0)$.

We choose two different frequencies, f_{c} equal to 1000 and 50 Hz, and plot the dispersion curves of $\hat{c}(f_{\mathrm{c}})$ and $1/\hat{Q}(f_{\mathrm{c}})$ of the poro-viscoacoustic model as the dotted and the dash-dot lines, respectively, in Figs 1 and 2. The dispersion values at the peak or central frequency

Table 2. Phase velocity c and specific quality factor Q dispersion values at the peak or central frequency.

Frequency (Hz)	Quality factor	Material A Quality factor	Velocity (m s^{-1})	Velocity (m s^{-1})
$f_p = 14788$	$Q(f_p) = 23$	$\hat{Q}(f_p) = 23$	$c(f_p) = 2957$	$\hat{c}(f_p) = 2867$
$f_c = 1000$	$Q(f_c) = 36$	$\hat{Q}(f_c) = 36$	$c(f_c) = 2856$	$\hat{c}(f_c) = 2843$
$f_c = 50$	$Q(f_c) = 111$	$\hat{Q}(f_c) = 111$	$c(f_c) = 2812$	$\hat{c}(f_c) = 2817$
		Material B		
$f_p = 4470$	$Q(f_p) = 10$	$\hat{Q}(f_p) = 10$	$c(f_p) = 2757$	$\hat{c}(f_p) = 2583$
$f_c = 1000$	$Q(f_c) = 12$	$\hat{Q}(f_c) = 12$	$c(f_c) = 2628$	$\hat{c}(f_c) = 2566$
$f_c = 50$	$Q(f_c) = 30$	$\hat{Q}(f_c) = 30$	$c(f_c) = 2474$	$\hat{c}(f_c) = 2498$

are shown in Table 2. This table and the two figures show that there is good agreement between the attenuation of the poro-viscoacoustic model and that of the double porosity model at the centre frequency f_c, but the agreement of the phase velocity depends on f_c. When f_c is near to f_p or the peak attenuation frequency of the double porosity model, the phase velocities $\hat{c}(f_c)$ and $c(f_c)$ are very different. However, f_p of material B (corresponding to sandstone at 10 m depth) is already 4470 Hz, and the f_p at larger depth will become much larger. So, for a seismic survey having frequencies typically less than 100 Hz, a Zener element still well approximates the double porosity sandstone. For example, Table 2 shows that the phase velocity difference between $\hat{c}(f_c)$ and $c(f_c)$ is less than 1 per cent for $f_c = 50$ Hz. In this case, f_c is much lower than f_p, and then the poro-viscoacoustic model can be confidently applied to successfully approximate the double porosity medium.

By the fact that a single Zener element produces good agreement in attenuation with that of the double porosity model at the centre frequency of the Zener element, we can infer that several Zener elements around the centre frequency of the source wavelet could make for excellent agreement of the attenuation with the double porosity in the narrow frequency band of the source wavelet. However, it is very hard to make a good match of the velocity dispersion between the two models if they are apparently different at the centre frequency of f_c. This means that if a single Zener element gives a significantly different velocity to that of the double porosity model at f_c, then several Zener elements with their centre frequencies around f_c will not to eliminate the difference. Therefore, this difference will limit the application of the poro-viscoacoustic model.

We have calculated 2-D analytical transient solutions of the average pressure wave p_c and the average fluid pressure wave p_f in homogeneous double porosity materials A and B and the corresponding poro-viscoacoustic model as well. Computations of waveforms were done for receiver distances of 283 and 849 m and a source centre frequency of 50 Hz and receiver distances of 14.1 and 42.3 m for a source centre frequency of 1000 Hz. For the 50 Hz source, the amplitudes of p_c and p_f were normalized to the peak value of p_c at a distance of 283 m; and for the 1000 Hz source, the normalization was with respect to peak values at a distance of 14.1 m.

Fig. 3 shows the $p_c$waveform (upper diagram) and the p_f waveform (lower diagram) with a source centre frequency of 50 Hz for material A. The corresponding waveforms for a source centre frequency of 1000 Hz are given in Fig. 4. The very good agreement between the double porosity model and the poro-viscoacoustic model means that the double porosity sandstone can be adequately approximated by the poro-viscoacoustic model with only one Zener element in both cases.

Fig. 5 shows the $p_c$waveform (upper diagram) and the p_f waveform (lower diagram) with a source centre frequency of 50 Hz for material B. Good agreement between the double porosity model and the viscoacoustic model only occurs for the lower frequency ($f_c =$ 50 Hz). However, for the source with $f_c = 1000$ Hz, the results, which are shown in Fig. 6, are very different from each other. In this case, the double porosity sandstone cannot be approximated by the poro-viscoacoustic medium.

Such a comparison provides a criterion for checking the validity of the approximations. If an acoustic wave in a heterogeneous double porosity medium needs to be numerically simulated through the approximation of the poroviscoacoustic model, then the source centre frequency should be much lower than the lowest peak attenuation frequency of every component making up the heterogeneous medium.

4 2-D NUMERICAL SOLUTION IN A HETEROGENEOUS MEDIUM

The previous treatment was for homogeneous media, for which we were able to derive analytic transient solutions. Now we consider heterogeneous models. First, we present the governing equations in time-domain form.

The linear transport laws eq. (3) can rewritten in the time domain as

$$-\nabla p_f = \rho_f \dot{\mathbf{v}} + F^{-1}(\eta/\kappa^*(\omega)) \times \dot{\mathbf{q}}, \tag{41}$$

where F^{-1}means inverse Fourier transformation. The convolution term in (41) represents Biot's attenuation and can also be approached by the introduction of relaxation functions and memory equations. For the sake of simplicity, only the low-frequency range will be considered in the numerical modelling. According to Biot (1962b), at low frequency (lower than Biot's relaxation frequency ω_c), the above equation can

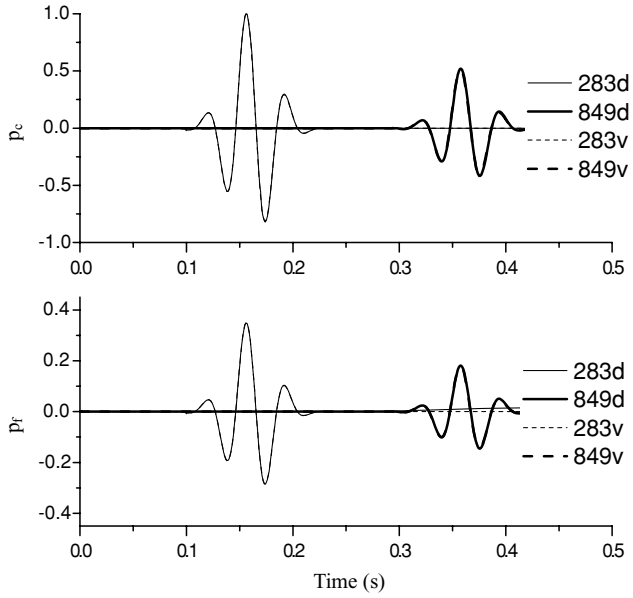

Figure 3. Analytical solution for pressures p_c (upper) and p_f (lower) of the double porosity model (solid line) and the poro-visco-acoustic model (dashed line) in material A. The source pulse has a centre frequency of 50 Hz. The numbers 283 and 849 denote the source–receiver distances of 283 and 849 m. The difference between the solid line and dashed line shows the effect of the approximation. At the same distance, the curves (dashed and solid lines) for both p_c and p_f show an almost perfect match.

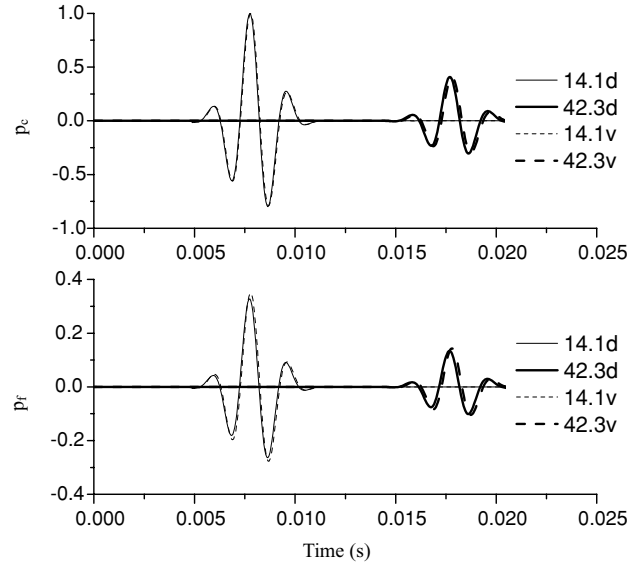

Figure 4. Analytical solution for pressures p_c (upper) and p_f (lower) of the double porosity model (solid line) and the poro-visco-acoustic model (dashed line) in material A. The source pulse has a centre frequency of 1000 Hz. The numbers 14.1 and 42.3 denote the source-receiver distances of 14.1 and 42.3 m. The difference between the solid line and the dashed line shows the effect of the approximation. At the same distance, the curves (dashed and solid lines) for both p_c and p_f show a good match.

be written as

$$-\nabla p_f = \rho_f \dot{\mathbf{v}} + m\dot{\mathbf{q}} + \frac{\eta}{\kappa_0^*}\mathbf{q}, \tag{42}$$

where $m = T\rho_f/\phi$; ϕ the overall porosity, κ_0^* the effective static permeability of the double porosity composite and T denotes the tortuosity (we assume $T \approx \phi^{-2\beta}$).

The conservation of linear momentum (eq. 5) can be written in the time domain as

$$\boldsymbol{\sigma}^D - \nabla p_c = \rho\dot{\mathbf{v}} + \rho_f\dot{\mathbf{q}}, \tag{43}$$

Eqs (2), (22), (42) and (43) constitute the poro-viscoelastic governing equations of double porosity media in the time domain.

Based on our previous findings, a single Zener element can well describe the double porosity medium under the condition that the centre frequency is much lower than the peak attenuation frequency. The wave in the heterogeneous double porosity medium can be solved

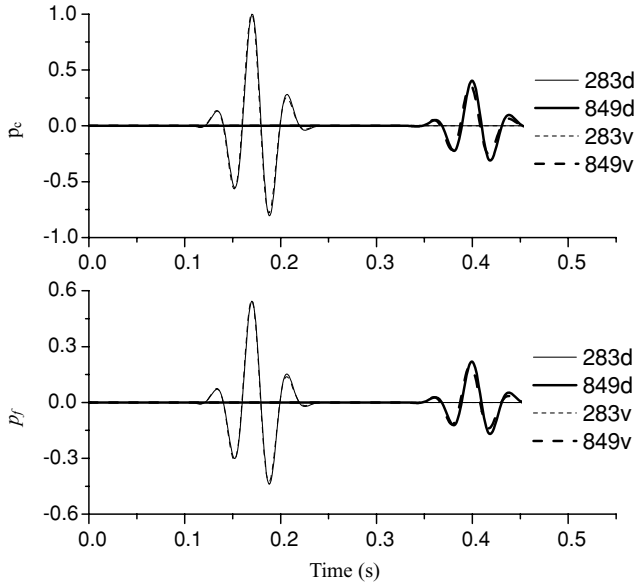

Figure 5. Analytical solution for pressure p_c(upper) and p f (lower) of the double porosity model (solid line) and the poro-viscoacoustic model (dashed line) in material B. The source pulse has a centre frequency of 50 Hz. The numbers 283 and 849 denote the source-receiver distances of 283 and 849 m. The difference between the solid line and the dashed line shows the effect of the approximation. At the same distance, the curves (dashed and solid lines) for both p_c and pf show a very good match.

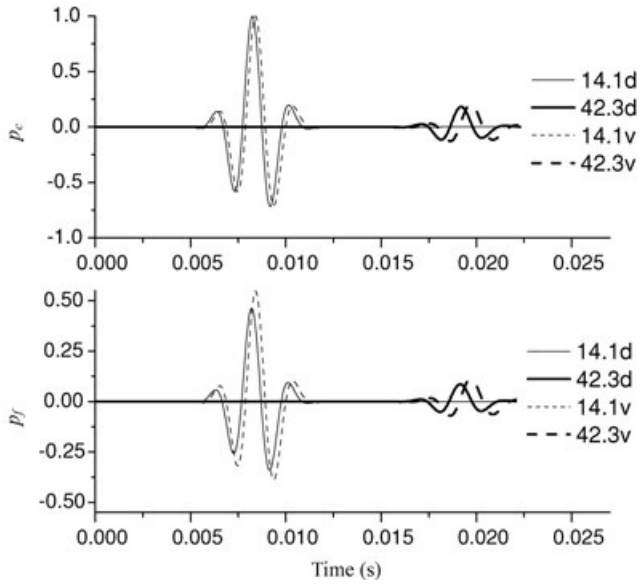

Figure 6. Analytical solution for pressures p_c (upper) and p_f (lower) of the double porosity model (solid line) and the poro-viscoacoustic model (dashed line) in material B. The source pulse has a centre frequency of 1000 Hz. The numbers 14.1 and 42.3 denote the source-receiver distances of 14.1 and 42.3 m. The difference between the solid line and the dashed line shows the effect of the approximation. At the same distance, the curves (dashed and solid lines) for both p_c and p_f show a poor match.

numerically by the poro-viscoelastic model. We apply relaxation functions of the Zener model to eqs. (22) to get two different sets of memory equations for the solid and the fluid, respectively; and if we choose a single relaxation function, the 2-D constitutive equations can be approximated as follows using three memory variables e^v, e^q and e^s(see Appendix B for details).

The governing equations can be written in matrix form as

$$\dot{\mathbf{F}} = \mathbf{MF} + \mathbf{S}, \tag{44}$$

where the quantity **F** is the field vector to be solved, given by

$$\mathbf{F} = \left[v_x, v_z, q_x, q_z, \boldsymbol{\sigma}_{xx}, \boldsymbol{\sigma}_{xz}, \boldsymbol{\sigma}_{zz}, p_f, e_{xx}, e^s, e_{zz}, e^q\right]. \tag{45}$$

The quantity **S** is the source vector, which can be written as

$$\mathbf{S} = \left[0, 0, 0, 0, s_{xx}, s_{xz}, s_{zz}, s_f, 0, 0, 0, 0\right]. \tag{46}$$

In eq. 44, the quantity **M** is the propagation matrix, which can be specified by the expanded form of eq. (44) as follows

$$\dot{v}_x = -\beta_{11}\partial_x p_{\rm c} - \beta_{12}\partial_x p_{\rm f} - \frac{\eta}{\kappa_0^*}\beta_{12} q_x, \tag{47}$$

$$\dot{v}_z = -\beta_{11}\partial_z p_{\rm c} - \beta_{12}\partial_z p_{\rm f} - \frac{\eta}{\kappa_0^*}\beta_{12} q_z, \tag{48}$$

$$\dot{q}_x = -\beta_{21}\partial_x p_{\rm c} - \beta_{22}\partial_x p_{\rm f} - \frac{\eta}{\kappa_0^*}\beta_{22} q_x, \tag{49}$$

$$\dot{q}_z = -\beta_{21}\partial_z p_{\rm c} - \beta_{22}\partial_z p_{\rm f} - \frac{\eta}{\kappa_0^*}\beta_{22} q_z, \tag{50}$$

$$\left.\begin{aligned}\dot{\boldsymbol{\sigma}}_{xx} = {} & \frac{1}{\tau_\sigma^p}\left[\left(1-\frac{\tau_\varepsilon^p}{\tau_\sigma^p}\right)\psi_{11}(\omega=0) + \frac{4}{3}\left(1-\frac{\tau_\varepsilon^s}{\tau_\sigma^p}\right)\psi_s(\omega=0)\right](v_{x,x}+v_{z,z}) \\ & -\frac{2}{\tau_\sigma^p}\left(1-\frac{\tau_\varepsilon^s}{\tau_\sigma^p}\right)\psi_s(\omega=0)v_{z,z} + \frac{1}{\tau_\sigma^p}\left(1-\frac{\tau_\varepsilon^p}{\tau_\sigma^p}\right)\psi_{12}(\omega=0)(q_{x,x}+q_{z,z}) + e_{xx} + s_{xx}\end{aligned}\right\}, \tag{51}$$

$$\dot{\boldsymbol{\sigma}}_{xz} = \frac{1}{\tau_\sigma^p}\left(1-\frac{\tau_\varepsilon^s}{\tau_\sigma^p}\right)\psi_s(\omega=0)(v_{x,z}+v_{z,x}) + e^s + s_{xz}, \tag{52}$$

$$\left.\begin{aligned}\dot{\boldsymbol{\sigma}}_{zz} = {} & \frac{1}{\tau_\sigma^p}\left[\left(1-\frac{\tau_\varepsilon^p}{\tau_\sigma^p}\right)\psi_{11}(\omega=0) + \frac{4}{3}\left(1-\frac{\tau_\varepsilon^s}{\tau_\sigma^p}\right)\psi_s(\omega=0)\right](v_{x,x}+v_{z,z}) \\ & -\frac{2}{\tau_\sigma^p}\left(1-\frac{\tau_\varepsilon^s}{\tau_\sigma^p}\right)\psi_s(\omega=0)v_{x,x} + \frac{1}{\tau_\sigma^p}\left(1-\frac{\tau_\varepsilon^p}{\tau_\sigma^p}\right)\psi_{12}(\omega=0)(q_{x,x}+q_{z,z}) + e_{zz} + s_{zz}\end{aligned}\right\}, \tag{53}$$

$$\dot{p}_f(t) = -\frac{1}{\tau^\sigma}\left(1-\frac{\tau^\varepsilon}{\tau^\sigma}\right)[\psi_{21}(\omega=0)(\partial_x v_x + \partial_z v_z) + \psi_{22}(\omega=0)(\partial_x q_x + \partial_z q_z] - e^q + s_f, \tag{54}$$

$$\left.\begin{aligned}\dot{e}_{xx} = {} & \frac{1}{\tau_\sigma^p}\left[\left(1-\frac{\tau_\varepsilon^p}{\tau_\sigma^p}\right)\psi_{11}(\omega=0) + \frac{4}{3}\left(1-\frac{\tau_\varepsilon^s}{\tau_\sigma^p}\right)\psi_s(\omega=0)\right](v_{x,x}+v_{z,z}) \\ & -\frac{2}{\tau_\sigma^p}\left(1-\frac{\tau_\varepsilon^s}{\tau_\sigma^p}\right)\psi_s(\omega=0)v_{z,z} + \frac{1}{\tau_\sigma^p}\left(1-\frac{\tau_\varepsilon^p}{\tau_\sigma^p}\right)\psi_{12}(\omega=0)(q_{1x,x}+q_{1z,z}) \\ & -\frac{1}{\tau_\sigma^p}e_{xx}\end{aligned}\right\}, \tag{55}$$

$$\dot{e}^s = \frac{1}{\tau_\sigma^p}\left(1-\frac{\tau_\varepsilon^s}{\tau_\sigma^p}\right)\psi_s(\omega=0)\left[v_{x,z}+v_{z,x}\right] - \frac{1}{\tau_\sigma^p}e_{sij}^l, \tag{56}$$

$$\left.\begin{aligned}\dot{e}_{zz} = {} & \frac{1}{\tau_\sigma^p}\left[\left(1-\frac{\tau_\varepsilon^p}{\tau_\sigma^p}\right)\psi_{11}(\omega=0) + \frac{4}{3}\left(1-\frac{\tau_\varepsilon^s}{\tau_\sigma^p}\right)\psi_s(\omega=0)\right](v_{x,x}+v_{z,z}) \\ & -\frac{2}{\tau_\sigma^p}\left(1-\frac{\tau_\varepsilon^s}{\tau_\sigma^p}\right)\psi_s(\omega=0)v_{x,x} + \frac{1}{\tau_\sigma^p}\left(1-\frac{\tau_\varepsilon^p}{\tau_\sigma^p}\right)\psi_{12}(\omega=0)(q_{1x,x}+q_{1z,z}) \\ & -\frac{1}{\tau_\sigma^p}e_{zz}\end{aligned}\right\}, \tag{57}$$

$$\dot{e}^q = \frac{1}{\tau^\sigma}\left(1-\frac{\tau^\varepsilon}{\tau^\sigma}\right)[\psi_{21}(\omega=0)(\partial_x v_x + \partial_z v_z) + \psi_{22}(\omega=0)(\partial_x q_x + \partial_z q_z)] - \frac{1}{\tau^\sigma}e^q. \tag{58}$$

Here, eqs (47)–(50) are obtained from eqs (42) and (43), the relaxation times τ^ε and τ^σ are determined by eq. (40), m is defined in eq. (42) and we also have

$$\begin{bmatrix}\beta_{11} & \beta_{12}\\ \beta_{21} & \beta_{22}\end{bmatrix} = \begin{bmatrix}-m & \rho_{\rm f}\\ \rho_{\rm f} & -\rho\end{bmatrix}\Big/\left(\rho_{\rm f}^2 - \rho m\right). \tag{59}$$

The stiff parts of the 2-D governing equations (47–50) are the terms with $\frac{\eta}{\kappa^*}\beta_{ij}q_{1l}$, which can be solved by a time splitting method (Carcione J.M. 1995, 1996); and the non-stiff parts can be solved by an explicit fourth-order Runge-Kutta method. The Fourier pseudo-spectral staggered-grid method is used to calculate the spatial derivatives (Carcione & Hellet 1999).

We will now consider two specific numerical examples using the same two-layer DPDP medium but apply poro-viscoacoustic and poro-viscoelastic models, respectively. The former numerical solution will be compared with the analytical solution of DPDP theory. The poro-viscoacoustic governing equations are obtained by ignoring the shear response (see Appendix B). A staggered grid of 258 × 258 points is used, and the source functions $\dot{S}$ and $\dot{S}_{\rm f}$ are taken to be Ricker-type wavelets, eq. (19), with a central frequency of 50 Hz. The two-layer heterogeneous 2-D model, shown in Fig. 7, has as its upper layer the double porosity material B, whose properties are listed in Table 1. To get a strong reflection, the lower layer is chosen as the Biot porous medium, which corresponds to the phase 1 sandstone at a depth of

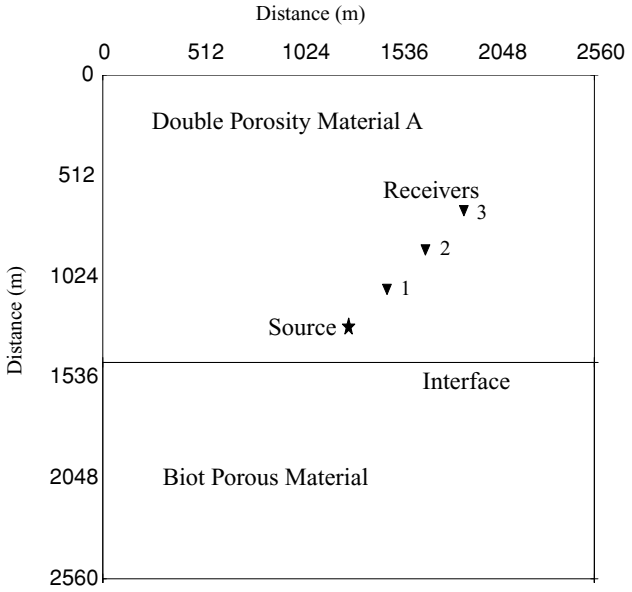

Figure 7. The 2-D model extends 2560 m in the horizontal and vertical directions and comprises two layers. The interface is at $Z = 1460$ m.The upper layer is the double porosity sandstone (Material A) and the lower layer is the Biot porous medium corresponding to phase 1 at 10 km depth. The source pulse has a centre frequency of 50 Hz. The distances are shown along the X and Z axes, with a grid spacing of 10 m. The source is located at (1280 m, 128 0m) and the three receivers denoted by numbers 1, 2 and 3 are at distances from the source of 283, 566 and 849 m, respectively.

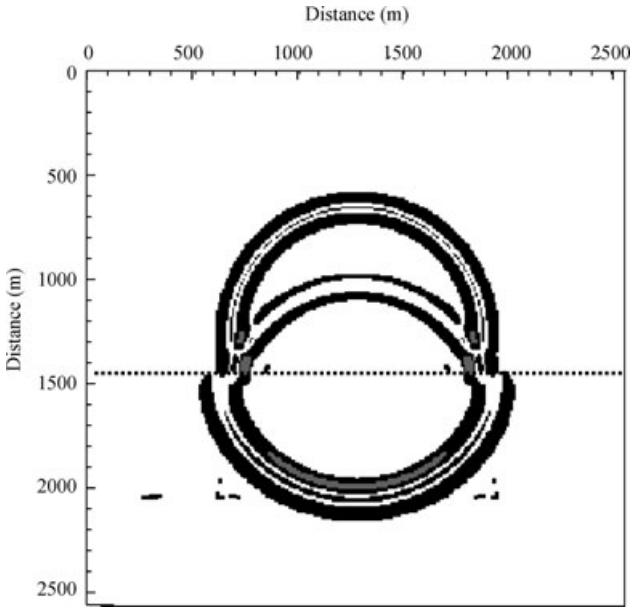

Figure 8. Snapshot of $p_c$wavefield at 300 ms in a two layer heterogeneous porous media. The upper layer is the double porosity sandstone (Material A) and the lower layer is a Biot porous medium corresponding to phase 1 at 10 km depth. The source pulse has a centre frequency of 50 Hz. The distances are shown along the X and Z axes, with a grid spacing of 10 m. The source is located at (1280 m, 1280 m) and the interface is at $Z = 1460$ m.

10 km by Walton theory (see Pride *et al.* 2004 for details). It has a porosity of 0.1, a permeability 1.0×10^{-16} m^2, a drained bulk modulus 2.925×10^{10} N m^{-2} and a shear modulus 3.04×10^{10}N m^{-2}. As a special case of the double porosity model, we set the volume fraction of phase 2, v_2, to be equal to zero. The Biot porous medium does not have the internal flow mechanism and the relaxation frequency of the Biot viscodynamic mechanism is set at $1.0 \times 10^{+8}$ Hz. So, both materials can be well described by the poro-viscoacoustic model for the source wave having a 50 Hz centre frequency. The source is located at the point $x = 1280$ m and $z = 1280$ m; the interface is at $z = 1460$ m. The wavefield snapshots of p_c and p_c at 300 ms are shown in Figs 8 and 9, respectively.

Both p_c and p_f show a strong reflection wave front, which is the result of the interface of the macroscopic heterogeneity. Fig. 9 shows that the p_f wave front has a similar pattern with that of p_c.However, the value of p_f around the source point remains very high, which means the double porosity model also has an average slow P wave, which was not explicitly discussed in this paper, but which arises in the numerical solution.

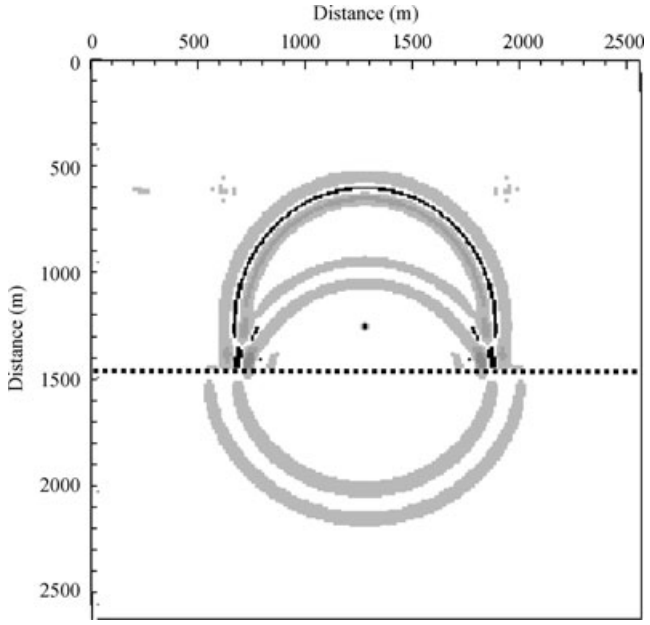

Figure 9. Snapshot of p_f wavefield at 300 ms in a two layer heterogeneous porous medium. The upper layer is the double porosity sandstone (Material A) and the lower layer is the Biot porous medium corresponding to phase 1 at 10 km depth. The source pulse has a centre frequency of 50 Hz. The distances are shown along the X and Z axes, with a grid spacing of 10 m. The source is located at (1280 m, 1280 m) and the interface is at $Z = 1460$ m.

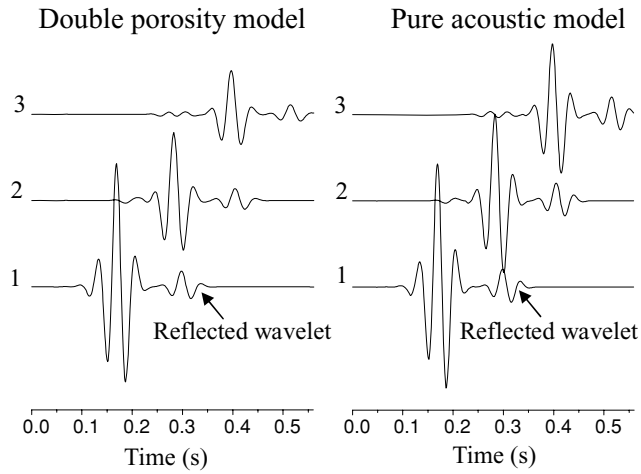

Figure 10. Comparison of the p_c waveforms for the double porosity model (left-hand side) and the corresponding pure acoustic model—no intrinsic attenuation (right-hand side). The amplitudes are normalized according to the maximum amplitude of receiver 1.

The high level attenuation in the double porosity material (upper layer) can be illustrated by the p_c waveform (see the left-hand side of Fig. 10) recorded by the three receivers located at distances of 283, 566 and 849 m from the source (see Fig. 7). The right-hand side of Fig. 10 shows the corresponding acoustic pressure waveform for a two-layer pure acoustic model (no intrinsic attenuation), having the same geometrical structure as our two-layer porous media. The layer densities of the pure acoustic model are equal to those of the porous model; whereas the two wave speeds of the pure acoustic model are the same as the velocities of the upper and lower porous layers at a frequency of 50 Hz . On the right-hand side of the figure, the change of maximum amplitude with distance from the source reflects pure geometrical spreading of the wave front and loss due to reflection of energy. Compared with the pure acoustic situation (right-hand side), the maximum amplitudes of the direct wave on the left-hand side of the figure (viscoacoustic case) significantly decrease with increasing distance. This indicates very strong attenuation caused by the local flow mechanism of the double porosity model.

Since material B forming the upper layer and the source–receiver distances for receivers designated 1 and 3 are the same as that in Fig. 5, we now compare the p_c waveform computed with our numerical method against the analytical p_c waveform of the poro-viscoacoustic model in Fig. 5 for a homogenous medium (note the good agreement between the double porosity model and the visco-acoustic model). Results are shown in Fig. 11. Apart from the reflected wavelet (in the inhomogeneous case), the normalized p_c waveforms at the same distances perfectly coincide. This clearly verifies the correctness of our numerical method and the computer code.

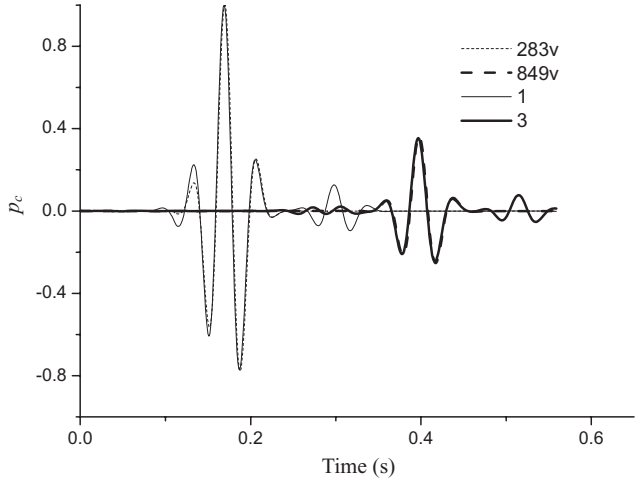

Figure 11. Comparison between the p_c waveforms for receivers 1, 3 (left-hand side of Fig. 10) and that for 283v, 849v (Fig. 5). Source–receiver distances are 283 and 849 m.

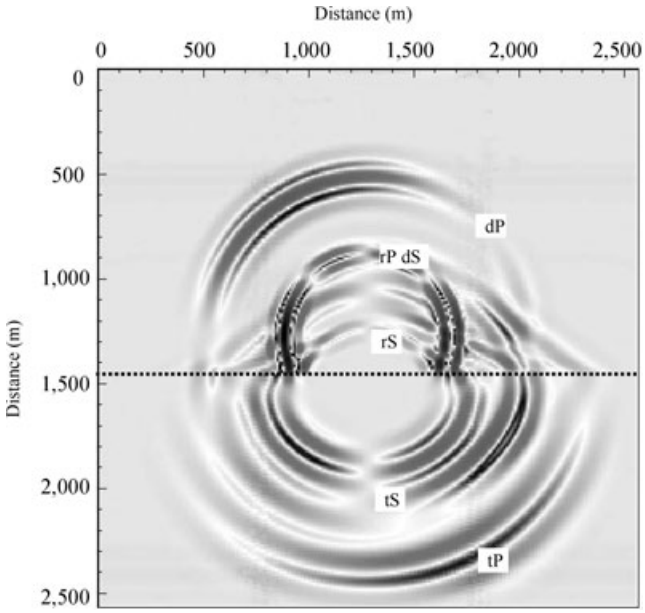

Figure 12. Snapshot of the rock-frame vertical particle velocity at 300 ms in a two layer heterogeneous poro-viscoelastic media. The upper layer and the lower layer are the same rocks shown as in Figs 8 and 9 (for the visco-acoustic case) but now having non-zero shear modulus (viscoelastic case). The source pulse has a centre frequency of 50 Hz. The distances are shown along X and Z axes, with a grid spacing of 10 m. The source is located at (1280 m, 1280 m) and the interface is at $Z = 1460$ m. Along the central vertical axis, from top to the bottom, there are six wave fronts corresponding to the direct P wave, the reflected P and the direct S waves(interfering), the reflected S wave, the transmitted S and P waves, which are denoted as dP, rP, dS, rS, tS and tP, respectively.

For the same rock model, we extend the solution for the poro-viscoacoustic model to poro-viscoelastic case, which takes account of the shear waves and therefore is more realistic. The shear wave relaxation times of the upper layer are chosen to be the same as those of the P wave. The source is chosen as

$$\mathbf{S} = [0, 0, 0, 0, 1, 1, 1, 1, 0, 0, 0, 0]\, f(t). \tag{60}$$

Here the pulse $f(t)$ is given in eq. (19) (from Carcione & Quiroga-Goode 1995).

To compare with the poro-viscoelastic wave patterns published by Carcione & Hellet (1999) and Carcione & Seriani (2001), we show in Fig. 12 the wavefield snapshot of the average solid particle velocity at a time of 300 ms. Shear waves including the direct, the reflected and the transmitted shear waves are clear, along with the reflected and the transmitted P waves. The refracted S and P waves are excited along the interface and form the head wave. The P waves in both the upper and lower layer are much faster that those in Figs 8 or 9. It is clear that the shear moduli increase the P-wave moduli over those the poro-viscoacoustic case in which the shear moduli were set to be zero.

5 CONCLUSIONS

In this paper, we have analytically solved for the phase velocity and inverse quality factor (attenuation) dispersion characteristics, as well as the analytical transient pressure waveform for a homogeneous acoustic double porosity model and for a poro-viscoacoustic model. By the method of fitting the relaxation times to the value of the quality factor of the double porosity model at the centre frequency of the Zener element, the suggested poro-viscoacoustic model with a single Zener element can be used for the transient solution of the wave in a double porosity model. The restriction, however, is that the centre frequency of the source wavelet is much lower than the relaxation frequency of the internal mesoscopic flow. At low frequency, the tail of the mesoscopic peak can be well approximated by one flank of the Zener peak. However, it is worth noting that a Kelvin–Voigt(KV) element as a replacement for the Zener element can be a better approximation in this case, since attenuation $1/Q$ of the KV element is proportional to frequency ω(Carcione 2007; Carcione *et al.* 2004)

We have extended the poro-viscoacoustic model to the poro-viscoelastic case, which incorporates shear waves and is therefore more realistic. For heterogeneous double porosity 2-D media, we obtained numerical transient solutions by means of poro-viscoelastic modeling, using a time splitting method for the non-stiff parts. We used an explicit fourth-order Runge-Kutta method for the time integration and a Fourier pseudospectral staggered-grid for handling the spatial derivative terms (Carcione J.M. 1995, 1996). For the same rock model, the poro-viscoacoustic solution is a special case of the poro-viscoelastic solution. Comparison with the analytical solution for a homogeneous model shows the correctness of this approach.

ACKNOWLEDGMENTS

This research was supported by grants from the Australian Research Council and the Swiss National Science Foundation. We thank the reviewers, Dr J Carcione and Dr E Saenger, for their constructive suggestions, which have improved the quality of the paper.

REFERENCES

Auriault, J.L., Borne, L. & Chambon, R., 1985. Dynamics of porous saturated media, checking of the generalized law of Darcy, *J. acoust. Soc. Am.,* **77,** 1641–1650.

Biot, M.A, 1956. Theory of propagation of elastic waves in a fluid-saturated porous solid, I: low-frequency range, *J. acoust. Soc. Am.,* **28**(2), 168–178.

Biot, M.A., 1962. Mechanics of deformation and acoustic propagation in porous media, *J. appl. Phys.,* **33**(4), 1482–1498.

Carcione, J.M., 1996. Wave propagation in anisotropic, saturated porous media: plane-wave theory and numerical simulation, *J. acoust. Soc. Am.,* **99**(5), 2655–2666.

Carcione, J.M., 1998. Viscoelastic effective rheologies for modelling wave propagation in porous media, *Geophys. Prospect.,* **46,** 249–270.

Carcione, J.M., 2007. *Wave Fields in Real Media: Wave Propagation in Anisotropic, Anelastic, Porous and Electromagnetic Media, Handbook of Geophysical Exploration, Seismic Exploration,* Second edition (Revised and Extended), **Vol. 38**, edsHelbig K. and Treitel, S., Elsevier Ltd, Oxford, UK, Amsterdam, The Netherlands.

Carcione, J.M., & Hellet, H.B., 1999. Numerical solution of the poroviscoelastic wave equation on a staggered mesh, *J. Comput. Physics,* **154**(2), 520–527

Carcione, J.M. & Quiroga-Goode, G., 1995. Some aspects of the physics and numerical modelling of Biot compressional waves, *J. Comput. Acoust.,* **3**(4), 261–280.

Carcione, J.M. & Quiroga-Goode, G., 1996. Full frequency-range transient solution for compressional waves in a fluid-saturated viscoacoustic porous medium, *Geophys. Prospect.,* **44,** 99–129.

Carcione, J.M. & Seriani, G., 2001. Wave simulation in frozen porous media, *J. Comput. Phys.,* **170,** 676–695.

Carcione, J.M., Herman, G.C. & Kroode, A.P.E.T., 2002. Seismic modelling, *Geophysics,* **67**(4), 1304–1325.

Carcione, J.M., Poletto, F. & Gei, D., 2004, 3-D wave simulation in anelastic meida using the Kelvin-Voigt constitutive equation, *J. Comput. Phys.,* **196,** 282–287.

Dutta, N.C. & Odé, H., 1979a. Attenuation and dispersion of compressional waves in fluid-filled porous rocks with partial gas saturation (White model), part I: Biot theory, *Geophysics,* **44**(11), 1777–1788.

Dutta, N.C. & Odé, H., 1979b. Attenuation and dispersion of compressional waves in fluid-filled porous rocks with partial gas saturation (White model), part II: results, *Geophysics,* **44**(11), 1789–1805.

Dvorkin, J., Nolen-Hoeksema, R. & Nur, A., 1994. The squirt-flow mechanism: macroscopic description, *Geophysics,* **59**(3), 428–438.

Gelinksy, S. & Shapiro, S.A., 1997. Dynamic-equivalent medium approach for thinly layered saturated sediments, *Geophys. J. Int.,* **128**(1), F1–F4.

Gurevich, B. & Lopatnikov, S.L., 1995. Velocity and attenuation of elastic waves in finely layered porous rocks, *Geophys. J. Int.,* **121**(3), 933–947.

Johnson, D.L., 2001. Theory of frequency dependent acoustics in patchy-saturated porous media, *J. acoust. Soc. Am.,* **110**(2), 682–694.

Johnson, D.L., Koplik, J. & Dashen, R., 1987. Theory of dynamic permeability and tortuosity in fluid-saturated porous media, *J. Fluid Mech.,* **176,** 397–402.

Jones, T.D., 1986. Pore fluids and frequency-dependent wave propagation in rocks, *Geophysics,* **51**(10), 1939–1953.

Pride, S.R. & Berryman, J.G., 2003a. Linear dynamics of double-porosity and dual-permeability materials, I: governing equations and acoustic attenuation, *Phys. Rev.,* **E 68** 036604, 1–10.

Pride, S.R. & Berryman, J.G., 2003b. Linear dynamics of double-porosity and dual-permeability materials, II: fluid transport equations, *Phys. Rev.,* **E 68** 036603, 1–10.

Pride, S.R., Berryman, J.G. & Harris, J.M., 2004. Seismic attenuation due to wave-induced flow, *J. Geophys. Res.,* **109,** B01201, 1–19.

White, J.E., 1975. Computed seismic speeds and attenuation in rocks with partial gas saturation, *Geophysics,* **40**(2), 224–232.

APPENDIX A: THE COEFFICIENTS a^*_{mn} OF THE DPDP CONSTITUTIVE EQUATIONS

The coefficients appearing in eq. (1) are defined by

$$\left.\begin{aligned} a^*_{11} &= a_{11} - \frac{\mathrm{i}\omega a_{13}^2}{\mathrm{i}\omega a_{33} - r(\omega)}, \quad a^*_{12} = a_{12} - a_{13}\frac{\mathrm{i}\omega a_{23} + r(\omega)}{\mathrm{i}\omega a_{33} - r(\omega)} \\ a^*_{22} &= a_{22} + a_{23} - (a_{23} + a_{33})\frac{\mathrm{i}\omega a_{23} + r(\omega)}{\mathrm{i}\omega a_{33} - r(\omega)} \end{aligned}\right\}. \tag{A1}$$

Here a_{mn} are the coefficients of the DPDP constitutive equations (given below) and $r(\omega)$ is the internal transport coefficient (Pride & Berryman 2003a; Pride *et al.* 2004).

$$\left.\begin{aligned} a_{11} &= \frac{1}{K^d}, \qquad a_{22} = \frac{v_1\alpha_1}{K_1^d}\left[\frac{1}{B_1} - \frac{\alpha_1(1-Q_1)}{1-K_1^d/K_2^d}\right] \\ a_{12} &= -\frac{v_1 Q_1}{K_1^d}\alpha_1, \quad a_{23} = -\frac{\alpha_1\alpha_2 K_1^d/K_2^d}{\left(1-K_1^d/K_2^d\right)^2}\left(\frac{1}{K^d} - \frac{v_1}{K_1^d} - \frac{v_2}{K_2^d}\right) \\ a_{13} &= -\frac{v_2 Q_2}{K_2^d}\alpha_2, \quad a_{33} = \frac{v_2\alpha_2}{K_2^d}\left(\frac{1}{B_2} - \frac{\alpha_2(1-Q_2)}{1-K_2^d/K_1^d}\right) \end{aligned}\right\}. \tag{A2}$$

The subscript 1 or 2 represents phase 1 or 2 and is shown by i in the following definition, K_i^d is the drained bulk modulus, v_i is the volume fraction, K^d is defined as the overall drained bulk modulus of the two-phase composite (the modulus defined in the quasi-static limit where the local fluid pressure throughout the composite is everywhere unchanged), and it is suggested to use the Hashin & Shtrikman (1963) bounds; Q_i are auxiliary constants given by

$$Q_i = \frac{1}{v_i}\frac{1-K_j^d/K^d}{1-K_j^d/K_i^d}, \; j \neq i, \tag{A3}$$

B_i is Skempton's coefficient (fluid-pressure change divided by confining-pressure change for a sealed sample) and may be determined from

$$B_i = \frac{1/K_i^d - 1/K_\mathrm{s}}{1/K_i^d - 1/K_\mathrm{s} + \phi_i\left(1/K_\mathrm{f} - 1/K_\mathrm{s}\right)}, \tag{A4}$$

where K_s is the bulk modulus of the grains, K_f is the bulk modulus of the fluid and ϕ_i is the porosity.

The quantity α_i is the Biot–Willis coefficient of phase i and may be determined from

$$\alpha_i = \left(1 - K_i^d/K_i^u\right)/B_i. \tag{A5}$$

Here $K_i^u$is Gassmann's undrained bulk modulus (confining-pressure change divided by sample dilatation for a sealed sample). It is given by

$$K_i^u = \frac{K_i^d}{1 - B_i(1 - K_i^d/K_\mathrm{s})}. \tag{A6}$$

The internal transport coefficient $r(\omega)$ was expressed by Pride & Berryman (2003a) and Pride *et al.* (2004) as

$$r(\omega) = r_m\sqrt{1 - \mathrm{i}\frac{\omega}{\omega_m}}, \tag{A7}$$

where, for the situations where the two phases have strong contrasts in their physical properties and if $k_1/k_2 << 1$,

$$r_m = -\frac{k_1 K_1^d}{\eta L_1^2}\left[\frac{a_{12} + B_0(a_{22}+a_{33})}{R_1 - B_0/B_1}\right]\left[1 + 0(k_1/k_2)\right]. \tag{A8}$$

In the above equation, R_1 is the ratio of the average static confining pressure in phase 1 to the pressure applied to the external surface of a sealed sample of the composite and is given by

$$R_1 = Q_1 + \frac{\alpha_1(1-Q_1)B_0}{1-K_1^d/K_2^d} - \frac{v_2}{v_1}\frac{\alpha_2(1-Q_2)B_0}{1-K_2^d/K_1^d}, \tag{A9}$$

The quantity B_0 is the static Skempton's coefficient for the composite and given by

$$B_0 = -\frac{(a_{12}+a_{13})}{a_{22}+2a_{23}+a_{33}}, \tag{A10}$$

The symbol L_1 stands for the characteristic length of the fluid pressure gradient. For a concentric sphere geometry, in which a sphere of phase 2 having a radius of a is embedded within a sphere of phase 1 having a radius of$R$, the characteristic length is given by

$$L_1^2 = \frac{9}{14}R^2\left[1 - \frac{7}{6}\frac{a}{R} + 0\left(a^3/R^3\right)\right]. \tag{A11}$$

ω_m is the transition frequency and is given by

$$\omega_m = \frac{\eta B_1 K_1^d}{k_1\alpha_1}\left(r_m\frac{V}{S}\right)^2\left(1 + \sqrt{\frac{k_1 B_2 K_2^d \alpha_1}{k_2 B_1 K_1^d \alpha_2}}\right), \tag{A12}$$

where V/S is the volume-to-surface ratio and S is the area of $\partial\Omega_{12}$ (the internal interface separating phase 1 and phase 2) in each volume V of the composite.

Letting $\omega \to \infty$, and $\omega \to 0$, we have the limiting frequency values that determine the values of $\psi_{mn}(t=\infty)$ and $\psi_{mn}(t=0^+)$ in the numerical calculations:

$$a_{11}^*(\infty) = a_{11} - \frac{a_{13}^2}{a_{33}}, a_{12}^*(\infty) = a_{12} - a_{13}\frac{a_{23}}{a_{33}}, a_{22}^*(\infty) = a_{22} - \frac{a_{23}^2}{a_{33}}, \tag{A13}$$

$$a_{11}^*(0) = a_{11}, a_{12}^*(0) = a_{12} + a_{13}, a_{22}^*(0) = a_{22} + 2a_{23} + a_{33}. \tag{A14}$$

APPENDIX B: THE MEMORY VARIABLES AND EQUATIONS

Carcione (2007) considered a parallel system with L standard linear solid elements or a so-called generalized Zener material. The relaxation functions of the standard linear solid model are given in eqs (24) and (25).

Differentiating eq. (24)

$$\partial_t \psi_{mn} = \breve{\psi}_{mn}\delta(t) + \partial_t \breve{\psi}_{mn} H(t). \tag{B1}$$

Then, the right-hand side of eq. (22) can expressed as

$$\left.\begin{aligned} \partial_t \psi_{m1} * \boldsymbol{\nabla}\cdot\mathbf{v} &= \int_{-\infty}^{t}\left[\breve{\psi}_{m1}(t-\tau) + \dot{\breve{\psi}}_{m1}(t-\tau)H(t-\tau)\right]\boldsymbol{\nabla}\cdot\mathbf{v}\,\mathrm{d}\tau \\ \partial_t \psi_{m2} * \boldsymbol{\nabla}\cdot\mathbf{q} &= \int_{-\infty}^{t}\left[\breve{\psi}_{m2}(t-\tau) + \dot{\breve{\psi}}_{m2}(t-\tau)H(t-\tau)\right]\boldsymbol{\nabla}\cdot\mathbf{q}\,\mathrm{d}\tau \end{aligned}\right\}. \tag{B2}$$

Here $m = 1, 2$ and the above equations can be rewritten as

$$\left.\begin{aligned} \partial_t \psi_{m1} * \boldsymbol{\nabla}\cdot\mathbf{v} &= \breve{\psi}_{m1}(t=0)\boldsymbol{\nabla}\cdot\mathbf{v} + \partial_t\breve{\psi}_{m1}(t)H(t) * \boldsymbol{\nabla}\cdot\mathbf{v} \\ \partial_t \psi_{m2} * \boldsymbol{\nabla}\cdot\mathbf{q} &= \breve{\psi}_{m2}(t=0)\boldsymbol{\nabla}\cdot\mathbf{q} + \partial_t\breve{\psi}_{m2}(t)H(t) * \boldsymbol{\nabla}\cdot\mathbf{q} \end{aligned}\right\}. \tag{B3}$$

The memory variable e_{mn} can be defined as

$$\left.\begin{aligned} e_{m1} &= \partial_t\breve{\psi}_{m1}(t)H(t) * \boldsymbol{\nabla}\cdot\mathbf{v} \\ e_{m2} &= \partial_t\breve{\psi}_{m2}(t)H(t) * \boldsymbol{\nabla}\cdot\mathbf{q} \end{aligned}\right\}. \tag{B4}$$

Then eq. (22) can be written as

$$-\begin{bmatrix}\dot{p}_c(t)\\ \dot{p}_f(t)\end{bmatrix} = \begin{bmatrix}\psi_{11}(t=0^+) & \psi_{12}(t=0^+)\\ \psi_{21}(t=0^+) & \psi_{22}(t=0^+)\end{bmatrix}\begin{bmatrix}\boldsymbol{\nabla}\cdot\mathbf{v}(t)\\ \boldsymbol{\nabla}\cdot\mathbf{q}(t)\end{bmatrix} + \begin{bmatrix}e_{11}+e_{12}\\ e_{21}+e_{22}\end{bmatrix}. \tag{B5}$$

To obtain the memory equations, e_{m1} can be extended (or integrated) as follows:

$$e_{m1} = \int_{-\infty}^{t}\partial_\tau\breve{\psi}_{m1}(\tau)H(\tau)\boldsymbol{\nabla}\cdot\mathbf{v}(t-\tau)\mathrm{d}\tau. \tag{B6}$$

Then, we have

$$e_{m1} = \int_{0^+}^{t}\partial_\tau\breve{\psi}_{m1}(\tau)\boldsymbol{\nabla}\cdot\mathbf{v}(t-\tau)\mathrm{d}\tau. \tag{B7}$$

Substituting eq. (25) into eq.(B4) gives

$$e_{m1} = \sum_{l=1}^{L_{i1}} e_{m1}^l, \tag{B8}$$

where

$$e_{m1}^l = \frac{\psi_{m1}(t=\infty)}{L_{m1}\tau_{m1}^{\sigma l}}\left(1 - \frac{\tau_{m1}^{\varepsilon l}}{\tau_{m1}^{\sigma l}}\right)\int_{0^+}^{t}\exp\left(-\frac{\tau}{\tau_{m1}^{\sigma l}}\right)\boldsymbol{\nabla}\cdot\mathbf{v}(t-\tau)\mathrm{d}\tau. \tag{B9}$$

The time derivative of (B9) gives the memory equation

$$\left.\begin{aligned} \partial_t e_{i1}^l = \frac{\psi_{m1}(t=\infty)}{L_{m1}\tau_{m1}^{\sigma l}}&\left(1 - \frac{\tau_{m1}^{\varepsilon l}}{\tau_{m1}^{\sigma l}}\right) \\ &\times\left[\int_{0^+}^{t}\exp\left(-\tfrac{\tau}{\tau_{m1}^{\sigma l}}\right)\partial_\tau\boldsymbol{\nabla}\cdot\mathbf{v}(t-\tau)\mathrm{d}\tau + \exp\left(-\tfrac{t}{\tau_{m1}^{\sigma l}}\right)\boldsymbol{\nabla}\cdot\mathbf{v}(t=0)\right] \end{aligned}\right\}. \tag{B10}$$

Integration by parts yields

$$\left.\begin{aligned} &\int_{0^+}^{t}\exp\left(-\frac{\tau}{\tau_{m1}^{\sigma l}}\right)\partial_t\boldsymbol{\nabla}\cdot\mathbf{v}(t-\tau)\mathrm{d}\tau \\ &\quad= -\exp\left(-\frac{t}{\tau_{m1}^{\sigma l}}\right)\boldsymbol{\nabla}\cdot\mathbf{v}(t=0) + \boldsymbol{\nabla}\cdot\mathbf{v}(t) \\ &\qquad -\frac{1}{\tau_{m1}^{\sigma l}}\int_{\tau=0^+}^{\tau=t}\exp\left(-\frac{\tau}{\tau_{m1}^{\sigma l}}\right)\boldsymbol{\nabla}\cdot\mathbf{v}(t-\tau)d\tau \end{aligned}\right\}. \tag{B11}$$

Eq. (B10) can then be rewritten as

$$\left.\begin{aligned}\partial_t e^l_{m1} = {} & \frac{\psi_{m1}(t=\infty)}{L_{m1}\tau^{\sigma l}_{m1}}\left(1-\frac{\tau^{\varepsilon l}_{m1}}{\tau^{\sigma l}_{m1}}\right)\\ & \times\left[\boldsymbol{\nabla}\cdot\mathbf{v}(t)-\frac{1}{\tau^{\sigma l}_{m1}}\int_{\tau=0^+}^{\tau=t}\exp\left(-\frac{\tau}{\tau^{\sigma l}_{m1}}\right)\boldsymbol{\nabla}\cdot\mathbf{v}(t-\tau)d\tau\right]\end{aligned}\right\}, \tag{B12}$$

or

$$\left.\begin{aligned}\partial_t e^l_{m1} = {} & \frac{\psi_{m1}(t=\infty)}{L_{m1}\tau^{\sigma l}_{m1}}\left(1-\frac{\tau^{\varepsilon l}_{m1}}{\tau^{\sigma l}_{m1}}\right)\boldsymbol{\nabla}\cdot\mathbf{v}(t)\\ & -\frac{1}{\tau^{\sigma l}_{m1}}\left[\frac{\psi_{m1}(t=\infty)}{L_{m1}\tau^{\sigma l}_{m1}}\left(1-\frac{\tau^{\varepsilon l}_{m1}}{\tau^{\sigma l}_{m1}}\right)\int_{\tau=0^+}^{\tau=t}\exp\left(-\frac{\tau}{\tau^{\sigma l}_{m1}}\right)\boldsymbol{\nabla}\cdot\mathbf{v}(t-\tau)d\tau\right]\end{aligned}\right\}. \tag{B13}$$

By (B9), we get the memory equation

$$\partial_t e^l_{m1} = \frac{\psi_{m1}(t=\infty)}{L_{m1}\tau^{\sigma l}_{m1}}\left(1-\frac{\tau^{\varepsilon l}_{m1}}{\tau^{\sigma l}_{m1}}\right)\boldsymbol{\nabla}\cdot\mathbf{v}-\frac{1}{\tau^{\sigma l}_{m1}}e^l_{m1}. \tag{B14}$$

A similar derivation yields

$$\partial_t e^l_{m2} = \frac{\psi_{m2}(t=\infty)}{L_{m2}\tau^{\sigma l}_{m1}}\left(1-\frac{\tau^{\varepsilon l}_{m2}}{\tau^{\sigma l}_{m2}}\right)\boldsymbol{\nabla}\cdot\mathbf{q}-\frac{1}{\tau^{\sigma l}_{m2}}e^l_{m2}. \tag{B15}$$

We now consider the deviatoric (or shear) constitutive equations.

By eq.(2), the shear relaxation function ψ_s is defined as

$$\dot{\boldsymbol{\sigma}}^D = \partial_t\psi_s * \left[\boldsymbol{\nabla}\mathbf{v}+(\boldsymbol{\nabla}\mathbf{v})^T-\frac{2}{3}\boldsymbol{\nabla}\cdot\mathbf{v}\mathbf{I}\right], \tag{B16}$$

$$\psi_s = \breve{\psi}_s H(t), \tag{B17}$$

$$\breve{\psi}_s = \psi_s(t=\infty)\left[1-\frac{1}{L_s}\sum_{l=1}^{L_s}\left(1-\frac{\tau^{\varepsilon l}_s}{\tau^{\sigma l}_s}\right)\exp\left(-\frac{t}{\tau^{\sigma l}_s}\right)\right], \tag{B18}$$

where $\psi_s(t=\infty)$ is the value of relaxation functions at infinite time; L_s is the number of standard linear solid elements of ψ_s and $\tau^{\varepsilon l}_s$ and $\tau^{\sigma l}_s$ are the relaxation times of the deviatoric average velocity and the stress of the solid phase.

A similar derivation as for (B5) gives in the viscoelastic case

$$\dot{\boldsymbol{\sigma}}^D_{ij} = \psi_s(t=0^+)\left[V_{i,j}+V_{j,i}-\frac{2}{3}V_{i,i}\delta_{ij}\right]+\sum_{l=1}^{L_s}e^l_{sij}, \tag{B19}$$

$$\dot{e}^l_{sij} = -\frac{1}{\tau^{\sigma l}_s}e^l_{sij}+\frac{\psi_s(t=\infty)}{L_s\tau^{\sigma l}_s}\left(1-\frac{\tau^{\varepsilon l}_s}{\tau^{\sigma l}_s}\right)\left[V_{i,j}+V_{j,i}-\frac{2}{3}V_{i,i}\delta_{ij}\right]\quad l=1,\ldots L_s. \tag{B20}$$

Multiplying both sides of $\dot{p}_c(t)$ in eq. (B5) with δ_{ij} and combining with eq.(B19) and using $\boldsymbol{\sigma}^D=\boldsymbol{\sigma}-p_c\mathbf{I}$ shows the constitutive relation for the total stress in the solid frame to be

$$\begin{aligned}\dot{\boldsymbol{\sigma}}_{ij} = {} & \left[\psi_{11}(t=0^+)v_{i,i}+\psi_{12}(t=0^+)q_{i,i}+\sum_{l=1}^{L_{11}}e^l_{11}+\sum_{l=1}^{L_{12}}e^l_{12}\right]\delta_{ij}\\ & +\psi_s(t=0^+)\left[v_{i,j}+v_{j,i}-\tfrac{2}{3}v_{i,i}\delta_{ij}\right]+\sum_{l=1}^{L_s}e^l_{sij}.\end{aligned} \tag{B21}$$

Now, the 2-D constitutive equations with the memory equations are approximated and specified from the equations derived above.

For the sake of simplicity, we choose the numbers L_{11}, L_{12} and L_s equal to 1, and set all stress relaxation times equal to the acoustic wave values $\tau^{\sigma 1}_{mn}=\tau^P_\sigma$ $(m, n = 1, 2)$. We do likewise for the strain relaxation times $\tau^{\varepsilon 1}_{mn}=\tau^p_\varepsilon$ $(m, n = 1, 2)$ because only one classic P-wave dissipation peak is present. We also assume $\tau^{\sigma 1}_s=\tau^P_\sigma$ just for simplicity and rewrite $\tau^{\varepsilon 1}_s=\tau^s_\varepsilon$, $e^1_{11}+e^1_{12}=e^v$; $e^1_{21}+e^1_{22}=e^q$; $e^v+e^s_{xx}=e_{xx}$, $e^v+e^s_{zz}=e_{zz}$, $e^1_{sxz}=e^s$. Then we obtain the following expressions:

$$\left.\begin{aligned}\dot{\boldsymbol{\sigma}}_{xx} = {} & \left[\psi_{11}(t=0^+)+\frac{4}{3}\psi_s(t=0^+)\right](v_{x,x}+v_{z,z})\\ & -2\psi_s(t=0^+)v_{z,z}+\psi_{12}(t=0^+)(q_{x,x}+q_{z,z})+e_{xx}\end{aligned}\right\}, \tag{B22}$$

$$\dot{\boldsymbol{\sigma}}_{xz} = \psi_s(t=0^+)(v_{x,z}+v_{z,x})+e^s, \tag{B23}$$

$$\left.\begin{aligned}\dot{\boldsymbol{\sigma}}_{zz} = {} & \left[\psi_{11}(t=0^+)+\frac{4}{3}\psi_s(t=0^+)\right](v_{x,x}+v_{z,z})\\ & -2\psi_s(t=0^+)v_{x,x}+\psi_{12}(t=0^+)(q_{x,x}+q_{z,z})+e_{zz}\end{aligned}\right\}, \tag{B24}$$

$$\dot{p}_{\mathrm{f}}(t) = -\psi_{21}(t=0^+)\boldsymbol{\nabla}\cdot\mathbf{v}(t)-\psi_{22}(t=0^+)\boldsymbol{\nabla}\cdot\mathbf{q}(t)-e^q, \tag{B25}$$

$$\left.\begin{aligned}\frac{\partial}{\partial t}e_{xx} = \frac{1}{\tau_\sigma^p}\Bigg[\left(1-\frac{\tau_\varepsilon^p}{\tau_\sigma^p}\right)\psi_{11}(t=\infty)+\frac{4}{3}\left(1-\frac{\tau_\varepsilon^s}{\tau_\sigma^p}\right)\psi_s(t=\infty)\Bigg](v_{x,x}+v_{z,z})\\ -\frac{2}{\tau_\sigma^p}\left(1-\frac{\tau_\varepsilon^s}{\tau_\sigma^p}\right)\psi_s(t=\infty)v_{z,z}+\frac{1}{\tau_\sigma^p}\left(1-\frac{\tau_\varepsilon^p}{\tau_\sigma^p}\right)\psi_{12}(t=\infty)(q_{x,x}+q_{z,z})\\ -\frac{1}{\tau_\sigma^p}e_{xx}\end{aligned}\right\}, \tag{B26}$$

$$\dot{e}^s = \frac{\psi_s(t=\infty)}{\tau_\sigma^p}\left(1-\frac{\tau_\varepsilon^s}{\tau_\sigma^p}\right)\left[V_{x,z}+V_{z,x}\right]-\frac{1}{\tau_\sigma^p}e^l_{sij}, \tag{B27}$$

$$\left.\begin{aligned}\frac{\partial}{\partial t}e_{zz} = \frac{1}{\tau_\sigma^p}\Bigg[\left(1-\frac{\tau_\varepsilon^p}{\tau_\sigma^p}\right)\psi_{11}(t=\infty)+\frac{4}{3}\left(1-\frac{\tau_\varepsilon^s}{\tau_\sigma^p}\right)\psi_s(t=\infty)\Bigg](v_{x,x}+v_{z,z})\\ -\frac{2}{\tau_\sigma^p}\left(1-\frac{\tau_\varepsilon^s}{\tau_\sigma^p}\right)\psi_s(t=\infty)v_{x,x}+\frac{1}{\tau_\sigma^p}\left(1-\frac{\tau_\varepsilon^p}{\tau_\sigma^p}\right)\psi_{12}(t=\infty)(q_{x,x}+q_{z,z})\\ -\frac{1}{\tau_\sigma^p}e_{zz}\end{aligned}\right\}, \tag{B28}$$

$$\dot{e}^q = \frac{1}{\tau^\sigma}\left(1-\frac{\tau^\varepsilon}{\tau^\sigma}\right)[\psi_{21}(t=\infty)(\partial_x v_x+\partial_z v_z)+\psi_{22}(t=\infty)(\partial_x q_x+\partial_z q_z)]-\frac{1}{\tau^\sigma}e^q. \tag{B29}$$

Substituting eqs. (32) and (33) into the above equations, we get eqs (51)–(58).

Ignoring the shear response leads to the viscoacoustic equations

$$\dot{p}_{\rm c} = -\psi_{11}(\infty)\frac{\tau^\varepsilon}{\tau^\sigma}(\partial_x v_x+\partial_z v_z)-\psi_{12}(\infty)\frac{\tau^\varepsilon}{\tau^\sigma}(\partial_x q_x+\partial_z q_z)-e^v, \tag{B30}$$

$$\dot{p}_{\rm f} = -\psi_{21}(\infty)\frac{\tau^\varepsilon}{\tau^\sigma}(\partial_x v_x+\partial_z v_z)-\psi_{22}(\infty)\frac{\tau^\varepsilon}{\tau^\sigma}(\partial_x q_x+\partial_z q_z)-e^q, \tag{B31}$$

$$\dot{e}^v = \frac{1}{\tau^\sigma}\left(1-\frac{\tau^\varepsilon}{\tau^\sigma}\right)[\psi_{11}(t=\infty)(\partial_x v_x+\partial_z v_z)+\psi_{12}(t=\infty)(\partial_x q_x+\partial_z q_z)]-\frac{1}{\tau^\sigma}e^v. \tag{B32}$$

The equation for e^q is the same as eq. (58).